Check for updates

View Article Online
View Journal

Nanoscale

Accepted Manuscript

This article can be cited before page numbers have been issued, to do this please use: Z. Zhang, V. Fung and G. Hu, *Nanoscale*, 2025, DOI: 10.1039/D4NR05013D.

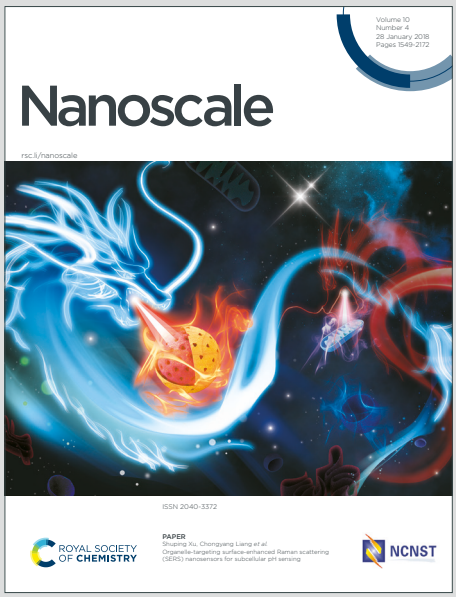

This is an Accepted Manuscript, which has been through the Royal Society of Chemistry peer review process and has been accepted for publication.

Accepted Manuscripts are published online shortly after acceptance, before technical editing, formatting and proof reading. Using this free service, authors can make their results available to the community, in citable form, before we publish the edited article. We will replace this Accepted Manuscript with the edited and formatted Advance Article as soon as it is available.

You can find more information about Accepted Manuscripts in the Information for Authors.

Please note that technical editing may introduce minor changes to the text and/or graphics, which may alter content. The journal's standard Terms & Conditions and the Ethical guidelines still apply. In no event shall the Royal Society of Chemistry be held responsible for any errors or omissions in this Accepted Manuscript or any consequences arising from the use of any information it contains.

ROYAL SOCIETY OF CHEMISTRY

rsc.li/nanoscale

View Article Online
DOI: 10.1039/D4NR05013D

Open Access Article. Published on 04 april 2025. Downloaded on 2025-04-13 20:33:42.
This article is licensed under a Creative Commons Attribution-NonCommercial 3.0 Unported Licence.

Pushing the Boundary of the Stability and Band Gap Pareto Front by Going Towards High-Entropy Perovskites

Zhendian Zhang[1], Victor Fung[2,*], Guoxiang Hu[1,3,*]

[1]School of Materials Science and Engineering, Georgia Institute of Technology, Atlanta, Georgia 30332, United States

[2]School of Computer Science and Engineering, Georgia Institute of Technology, Atlanta, Georgia 30332, United States

[3]School of Chemistry and Biochemistry, Georgia Institute of Technology, Atlanta, Georgia 30332, United States

Email: victorfung@gatech.edu, emma.hu@mse.gatech.edu.

Nanoscale Accepted Manuscript

ABSTRACT

Lead-free Cs_2BX_6 (B = Zr^{4+}, Sn^{4+}, Te^{4+}, Hf^{4+}, Re^{4+}, Os^{4+}, Ir^{4+}, Pt^{4+}, and X = Cl^-, Br^-, I^-) vacancy-ordered double perovskites have gained significant attention due to their high performance in solar cell devices. Besides mitigating toxicity concerns associated with the use of lead, the presence of formally tetravalent B site in Cs_2BX_6 has been demonstrated to improve the stability against air and moisture. Recently, experimental studies showed that high-entropy forms of the vacancy-ordered double perovskites can be synthesized and stabilized at room temperature, which opens new opportunities to design better solar cell absorbers. In this work, we employ high throughput density functional theory (DFT) calculations using the HSE06 hybrid functional to study 546 medium-to-high-entropy vacancy-ordered double perovskites. Our results show that $Cs_2\{B_1B_2B_3B_4\}_1X_6$ and $Cs_2\{B_1B_2B_3B_4\}_1\{XX'\}_6$ perovskites can break the existing linear scaling relationships between the bandgap and formation energy observed in the pure Cs_2BX_6 and $Cs_2B\{XX'\}_6$ perovskites, which enables materials which simultaneously

View Article Online
DOI: 10.1039/D4NR05013D

Open Access Article. Published on 04 april 2025. Downloaded on 2025-04-13 20:33:42.
This article is licensed under a Creative Commons Attribution-NonCommercial 3.0 Unported Licence.

exhibit an optimal band gap of ~1.3 eV for single junction solar cell along with a low formation energy. Electronic structure analysis reveals that this can be attributed to the weak coupling between the BX_6 octahedra in $Cs_2\{B_1B_2B_3B_4\}_1X_6$ and $Cs_2\{B_1B_2B_3B_4\}_1\{XX'\}_6$. Based on these findings, we identify analytical equations which can be used to efficiently predict the band gap and formation energy of high-entropy perovskites from their constituent pure perovskites. Our study offers simple and practical guidelines for the design and synthesis of novel high-entropy perovskites with improved photovoltaic performance.

INTRODUCTION

Lead halide perovskites are at present the best performing solution-processed photovoltaic materials, with a power conversion efficiency record of 26.7% in single junction perovskite solar cell and 34.6% in perovskite/Si 2T tandem in 2024.[1–5] However, the ultimate commercialization of these materials still faces serious practical challenges due to their toxicity from lead, and their instability against moisture, air, and temperature.[6–10] Alternative compositional and structural derivatives of the perovskite family have consequently been explored to assess their potential in photovoltaic applications.[11–16] Among these novel perovskites developed over the past decade, Cs_2BX_6 (B = Zr^{4+}, Sn^{4+}, Te^{4+}, Hf^{4+}, Re^{4+}, Os^{4+}, Ir^{4+} , Pt^{4+}, and X = Cl^-, Br^-, I^-) vacancy-ordered double perovskites have attracted particular attention following the recent demonstrations of their high performance in solar cell devices.[17–21] Besides mitigating toxicity concerns associated with the use of lead, the presence of formally tetravalent B site in Cs_2BX_6 can also improve air and moisture stability relative to the divalent B site in conventional $CsBX_3$ perovskites.[22–24]

High-entropy halide perovskites are an emerging class of materials that combine the intriguing properties of halide perovskites with the concept of high-entropy.[25,26] Common

Nanoscale Accepted Manuscript

View Article Online
DOI: 10.1039/D4NR05013D

Open Access Article. Published on 04 april 2025. Downloaded on 2025-04-13 20:33:42.
This article is licensed under a Creative Commons Attribution-NonCommercial 3.0 Unported Licence.

advantages of high-entropy materials, which contain five or more different elements distributed in a single crystal structure, include entropic stabilization (under high temperature) and a tunable continuum of materials properties.[25,27–29] This innovative design strategy has been widely explored in metals and oxides,[30–33] but its application to halide perovskites is a relatively new concept and holds great untapped potential. A recent experimental study has demonstrated a viable route to synthesize and stabilize high-entropy vacancy-ordered double perovskites at room temperature such as the five-element $Cs_2\{SnTeReIrPt\}_1Cl_6$ and six-element $Cs_2\{SnTeReOsIrPt\}_1Cl_6$ compositions.[25] This opens up new opportunities to design novel materials based on high-entropy vacancy-ordered double perovskites for photovoltaic devices beyond the state-of-the-art lead halide perovskites.

In this work, we performed high throughput density functional theory (DFT) calculations using the hybrid functional HSE06 to study over five hundred medium-to-high-entropy vacancy-ordered double perovskites. We calculated the band gap and formation energy of these perovskites and found that high-entropy perovskites exhibit emerging properties which are not present in their pure counterparts. We further analyzed their density of states (DOS) and revealed that this can be attributed to the unique electronic structure of vacancy-ordered double perovskites with weakly coupled octahedra. Finally, we identified the analytical equations which can be applied to efficiently predict the band gap and formation energy of high-entropy perovskites using the values of their constituent pure perovskites. Our work demonstrated new opportunities for applications of high-entropy halide perovskites in solar cell devices.

Nanoscale Accepted Manuscript

View Article Online
DOI: 10.1039/D4NR05013D

Open Access Article. Published on 04 april 2025. Downloaded on 2025-04-13 20:33:42.
This article is licensed under a Creative Commons Attribution-NonCommercial 3.0 Unported Licence.

RESULTS AND DISCUSSION

Vacancy-ordered double perovskites are a specialized class of perovskite materials in which specific atomic sites within the crystal structure are deliberately left vacant, leading to a unique arrangement of atoms. In conventional $Cs_2BB'X_6$ (B = Cu^+, Ag^+, Au^+, K^+, In^+, Ti^+, and B′= Bi^{3+}, Sb^{3+}, Tl^{3+}) double perovskites, two different cations B and B' occupy alternating positions within the lattice. However, in Cs_2BX_6 vacancy-ordered double perovskites, as shown in Figure 1, one of the cation sites is left vacant, creating a pattern of missing atoms within the structure. In this work, we considered 8 elements (Zr, Hf, Re, Os, Ir, Pt, Sn and Te) at the B site, and 3 elements (Cl, Br, and I) at the X site. Besides the pure Cs_2BX_6 perovskites, we also investigated three types of mixed perovskites: (1) $Cs_2B\{XX'\}_6$ with the X site mixed, (2) $Cs_2\{B_1B_2B_3B_4\}_1X_6$ with the B site mixed, and (3) $Cs_2\{B_1B_2B_3B_4\}_1\{XX'\}_6$ with both B and X sites mixed. For the X site mixing, we examined the combinations of Cl_4Br_2, Cl_2Br_4, Br_4I_2, and Br_2I_4, considering the atomic radii and structural symmetry.[25,34] Previous studies have shown that the large difference in atomic radii between Cl^- and I^- anions leads to low ionic miscibility, preventing Cl^- from substituting into the I^- lattice, particularly for relatively high concentration levels.[35–37] This in total yields 546 perovskite structures: (1) 24 pure Cs_2BX_6 perovskites (8 elements at the B site × 3 elements at the X site), (2) 32 $Cs_2B\{XX'\}_6$ perovskites (8 elements at the B site × 4 combinations at the X site), (3) 210 $Cs_2\{B_1B_2B_3B_4\}_1X_6$ perovskites (70 combinations at the B site × 3 elements at the X site), and (4) 280 $Cs_2\{B_1B_2B_3B_4\}_1\{XX'\}_6$ perovskites (70 combinations at the B site × 4 combinations at the X site).

Nanoscale Accepted Manuscript

View Article Online
DOI: 10.1039/D4NR05013D

Open Access Article. Published on 04 april 2025. Downloaded on 2025-04-13 20:33:42.
This article is licensed under a Creative Commons Attribution-NonCommercial 3.0 Unported Licence.

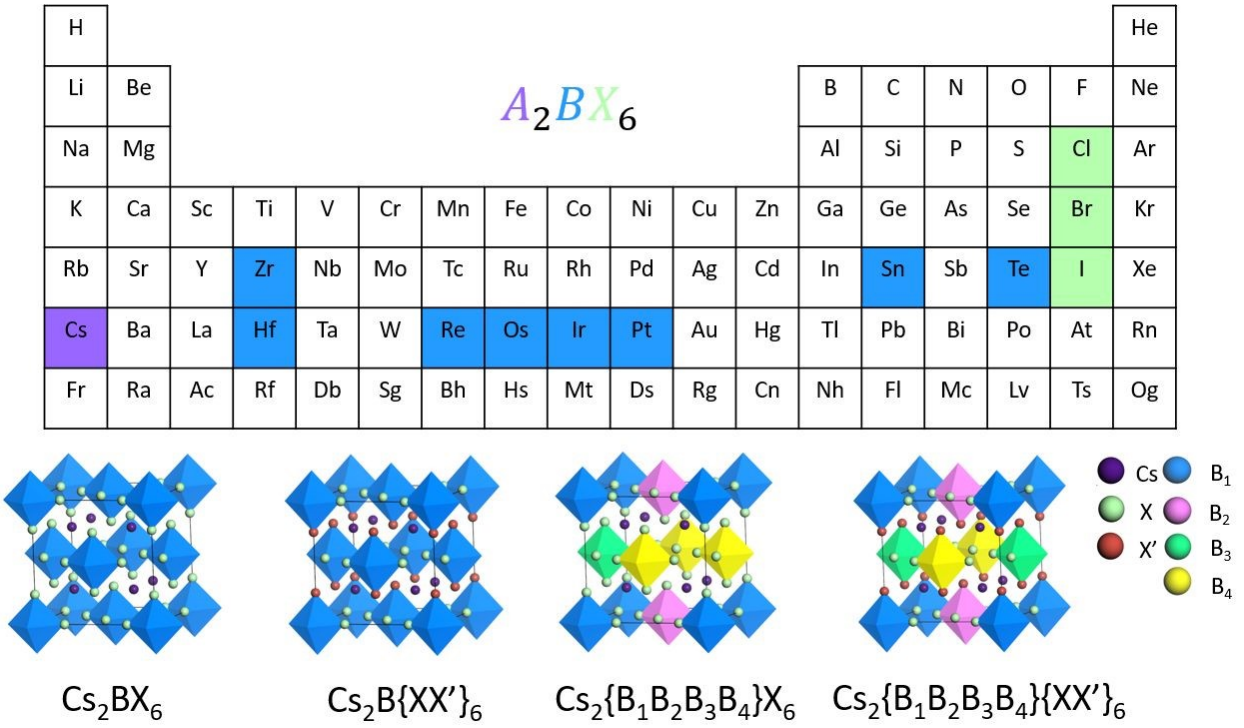

Figure 1. The chemical space and atomic structures of pure and mixed vacancy-ordered double perovskites investigated in this work.

Figure 2 presents the DFT-calculated formation energy and band gap for the 546 vacancy-ordered double perovskites. The computed values for the lattice constant, band gap, formation enthalpy, entropy, and Gibbs free energy at 298 K are provided in Table S1. A linear scaling relationship between them can be observed for Cs_2BX_6 and $Cs_2B\{XX'\}_6$ perovskites: the band gap increases as the magnitude of the formation energy increases. This has been widely reported for vacancy-ordered double perovskites, and can be roughly explained by the molecular orbital theory.[38–40] Typically, perovskites with stronger chemical (covalent) bonds have more negative formation energies (i.e. larger magnitude) along with a wider splitting between the bonding and anti-bonding molecular orbitals (i.e. larger band gap). As a result, perovskites with desirable band gaps (1.1 - 1.5 eV)[41] for light absorption normally exhibit relatively poor

Nanoscale Accepted Manuscript

View Article Online
DOI: 10.1039/D4NR05013D

Open Access Article. Published on 04 april 2025. Downloaded on 2025-04-13 20:33:42.
This article is licensed under a Creative Commons Attribution-NonCommercial 3.0 Unported Licence.

stabilities. As highlighted by a grey box in Figure 2, only very few Cs_2BX_6 and $Cs_2B\{XX'\}_6$ perovskites are in this band gap range, and their formation energy are relatively high, corresponding to low stability. Table 1 lists the chemical composition, band gap, and formation energy for these perovskites. Our computational predictions of the band gaps agree very well with previous computational and experimental studies.[22,40,42–44] It is also worth noting that all these perovskites are made of expensive metals (i.e., Pt, Os, or Ir). However, very excitingly, we found that the B site mixed $Cs_2\{B_1B_2B_3B_4\}_1X_6$ and $Cs_2\{B_1B_2B_3B_4\}_1\{XX'\}_6$ medium-to-high-entropy perovskites can break the linear scaling relationship between the formation energy and band gap, allowing for significantly more candidates exhibiting optimal band gap and high stability for solar absorbers.

Table S2 presents 99 promising vacancy-ordered double perovskites with band gaps ranging from 1.1 to 1.5 eV. It is important to highlight that, as solar-absorbing materials, these perovskites may exhibit dipole-allowed transition gaps (referred to as "allowed gaps") that are larger than their direct band gaps.[45] For example, the direct band gap of Cs_2SnI_6 was calculated to be 0.7 eV, while its dipole-allowed transition gap was found to be 1.1 eV. Additionally, these materials may exhibit significant exciton binding energies, which can impede charge separation and reduce open-circuit voltages in solar cells.[46] Therefore, in addition to the fundamental band gaps (VBM-CBM) shown in Figure 2, it is crucial to further investigate the optical band gap and exciton binding energy of these promising candidates in future studies. Moreover, while formation energy provides an initial estimate of the stability of predicted perovskites, phonon calculations and finite-temperature molecular dynamics simulations can be further employed for a more comprehensive evaluation of their dynamical and thermodynamic stability.

Nanoscale Accepted Manuscript

View Article Online
DOI: 10.1039/D4NR05013D

Open Access Article. Published on 04 april 2025. Downloaded on 2025-04-13 20:33:42.
This article is licensed under a Creative Commons Attribution-NonCommercial 3.0 Unported Licence.

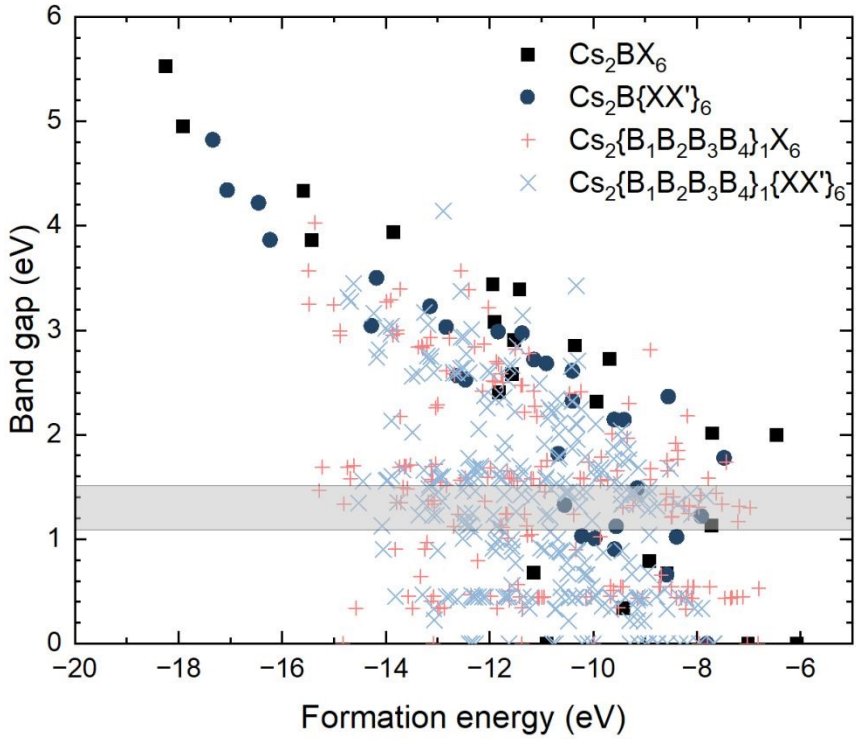

Figure 2. DFT calculated formation energy and band gap for 546 vacancy-ordered double perovskites including Cs_2BX_6, $Cs_2B\{XX'\}_6$, $Cs_2\{B_1B_2B_3B_4\}_1X_6$, and $Cs_2\{B_1B_2B_3B_4\}_1\{XX'\}_6$.

Table 1. The band gap E_g and formation energy E_f for the five Cs_2BX_6 and $Cs_2B\{XX'\}_6$ perovskites with 1.1 – 1.5 eV band gap.

	Cs_2PtI_6	**$Cs_2PtBr_4I_2$**	**$Cs_2OsCl_2Br_4$**	**$Cs_2OsBr_4I_2$**	**$Cs_2IrCl_4Br_2$**
E_g (eV)	1.13	1.49	1.12	1.22	1.33
E_f (eV)	-7.72	-9.15	-9.55	-7.91	-10.55

We then sought to understand the origin of the breaking of the linear scaling relationship between the formation energy and band gap for the B site mixed $Cs_2\{B_1B_2B_3B_4\}_1X_6$ perovskites. As shown in Figure 3a, we found that the formation energy of $Cs_2\{B_1B_2B_3B_4\}_1X_6$ can be predicted very well by the average of the formation energy of the constituent pure perovskites using the following equation:

Nanoscale Accepted Manuscript

View Article Online
DOI: 10.1039/D4NR05013D

Open Access Article. Published on 04 april 2025. Downloaded on 2025-04-13 20:33:42.
This article is licensed under a Creative Commons Attribution-NonCommercial 3.0 Unported Licence.

$$E_{form}(B_1,B_2,B_3,B_4) = \frac{1}{4}\sum_{i=1}^{4} E_{form}(B_i)$$

where $E_{form}(B_1, B_2, B_3, B_4)$ is the formation energy of $Cs_2\{B_1B_2B_3B_4\}_1X_6$, and $E_{form}(B_i)$ is the formation energy of the constituent pure perovskite. Whereas for the band gap, the corresponding equation does not work:

$$E_g(B_1,B_2,B_3,B_4) = \frac{1}{4}\sum_{i=1}^{4} E_g(B_i)$$

where $E_g(B_1, B_2, B_3, B_4)$ is the band gap of $Cs_2\{B_1B_2B_3B_4\}_1X_6$, and $E_g(B_i)$ is the band gap of the constituent pure perovskite. As illustrated in Figure 3b, equation (2) generally overestimates the band gap of $Cs_2\{B_1B_2B_3B_4\}_1X_6$ with the predicted values consistently exceeding those calculated using DFT.

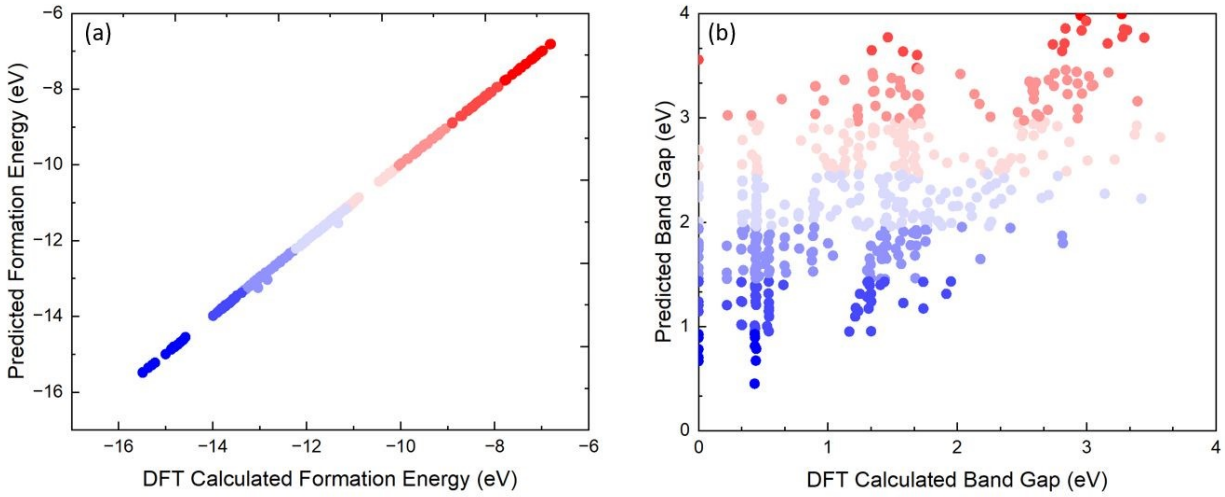

Figure 3 The comparison between (a) the predicted formation energy from equation (1) and the DFT calculated formation energy, and (b) the predicted band gap from equation (2) and the DFT calculated band gap.

The dramatically different correlations with the constituent pure perovskites for the formation energy and band gap shown in Figure 3 explain the breaking of the scaling observed in Figure 2. To get a better understanding of the correlation of the band gap of $Cs_2\{B_1B_2B_3B_4\}_1X_6$

Nanoscale Accepted Manuscript

View Article Online
DOI: 10.1039/D4NR05013D

Open Access Article. Published on 04 april 2025. Downloaded on 2025-04-13 20:33:42.
This article is licensed under a Creative Commons Attribution-NonCommercial 3.0 Unported Licence.

with their constituent pure perovskites, we performed a detailed analysis of their electronic structures. We found that for the diamagnetic metal ions (i.e., Hf^{4+}, Pt^{4+}, Sn^{4+}, Te^{4+}, and Zr^{4+}), the projected density of states is very similar in the mixed $Cs_2\{B_1B_2B_3B_4\}_1X_6$ and pure Cs_2BX_6 perovskites. This also applies to the paramagnetic metal ion Re^{4+} with each t_{2g} orbital being singly occupied (Figure 4a). As for the paramagnetic metal ions Ir^{4+} and Os^{4+}, we found that the pure perovskites exhibit degenerate t_{2g} orbitals (i.e., d_{xz},d_{yz}, and d_{xy} orbitals), which agrees with previous reports.[47–49] However, as shown in Figures 4b and 4c, in the mixed perovskites, the breaking of the symmetry leads to a splitting of the t_{2g} orbitals. It is noted that while the t_{2g} orbitals are different for the mixed and pure perovskites, the energy range of the projected density of states is not significantly changed.

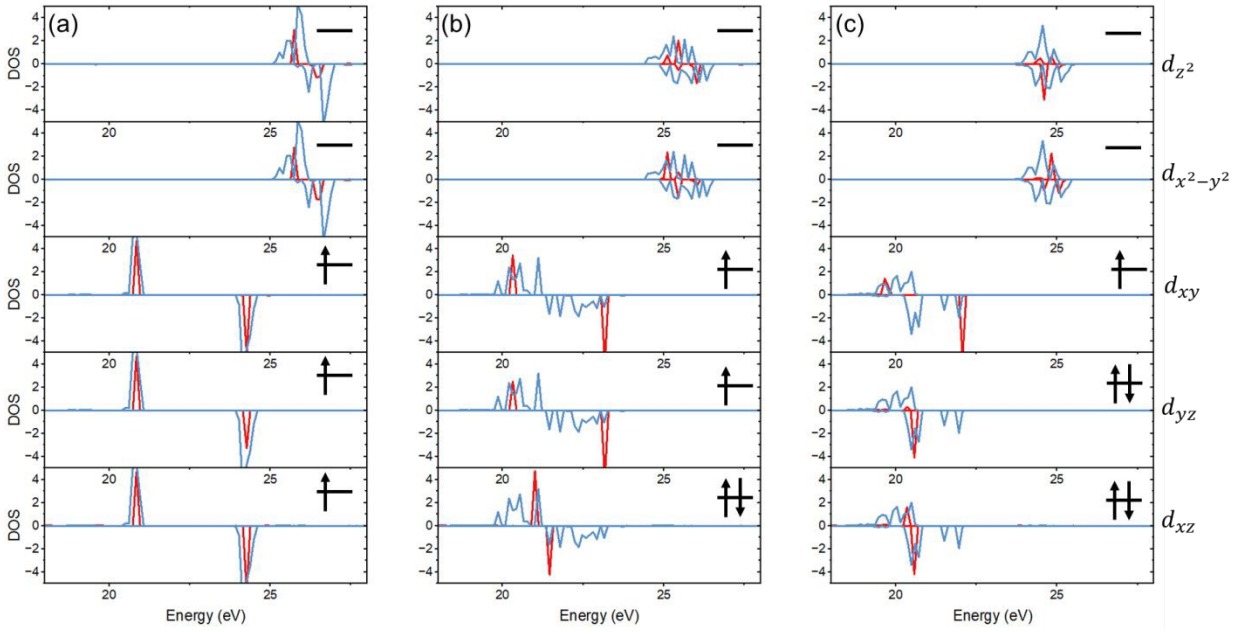

Figure 4 (a) Comparison of the projected density of states on Re 5*d* orbitals in $CsReCl_6$ (blue) and $Cs_2\{ZrSnRePt\}_1Cl_6$ (red). (b) Comparison of the projected density of states on Os 5*d* orbitals in $CsOsCl_6$ (blue) and $Cs_2\{ZrSnOsPt\}_1Cl_6$ (red). (c) Comparison of the projected density of states on Ir 5*d* orbitals in $CsIrCl_6$ (blue) and $Cs_2\{ZrSnIrPt\}_1Cl_6$ (red).

Nanoscale Accepted Manuscript

View Article Online
DOI: 10.1039/D4NR05013D

Open Access Article. Published on 04 april 2025. Downloaded on 2025-04-13 20:33:42.
This article is licensed under a Creative Commons Attribution-NonCommercial 3.0 Unported Licence.

The highly overlapped energy range of the electronic states in the pure and B-site-mixed perovskites shown in Figure 4 can be attributed to the relatively weak coupling between the neighboring BX_6 octahedra in vacancy-ordered double perovskites. Consequently, the conduction band minimum (CBM) and valence band maximum (VBM) of the pure perovskites can be used to estimate the band gap of the B-site-mixed perovskites. Figure 5 shows the alignment of the density of states between the B-site-mixed and the constituent pure perovskites using $Cs\{ZrSnTeHf\}_1Cl_6$ as an example. As one can see, the band gap of a B-site-mixed perovskite is essentially determined by the highest VBM and lowest CBM of the constituent pure perovskites, as expressed by the following equation:

$$E_{gap}(B_1,B_2,B_3,B_4) = \min(CBM_{B_1},CBM_{B_2},CBM_{B_3},CBM_{B_4}) - \max(VBM_{B_1},VBM_{B_2},VBM_{B_3},VBM_{B_4}) \quad (3)$$

where $E_{gap}(B_1, B_2, B_3, B_4)$ is the band gap of the B-site-mixed perovskite. CBM_{Bi} refers to the CBM, and VBM_{Bi} refers to the VBM of the constituent pure perovskites, respectively (i = 1, 2, 3, and 4). We further analyzed the 99 promising vacancy-ordered double perovskites listed in Table S2. Notably, 94 of them contain either Ir or Os, indicating that these two elements are particularly beneficial for achieving the desired band gap. This can be attributed to the unique band edges of $CsIrCl_6$ and $CsOsCl_6$. As shown in Figure S1, $CsIrCl_6$ exhibits the lowest CBM, while $CsOsCl_6$ has the highest VBM among the eight constituent pure perovskites. The desired band gap of 1.1–1.5 eV can only be achieved when either Ir or Os is present.

Nanoscale Accepted Manuscript

View Article Online
DOI: 10.1039/D4NR05013D

Open Access Article. Published on 04 april 2025. Downloaded on 2025-04-13 20:33:42.
This article is licensed under a Creative Commons Attribution-NonCommercial 3.0 Unported Licence.

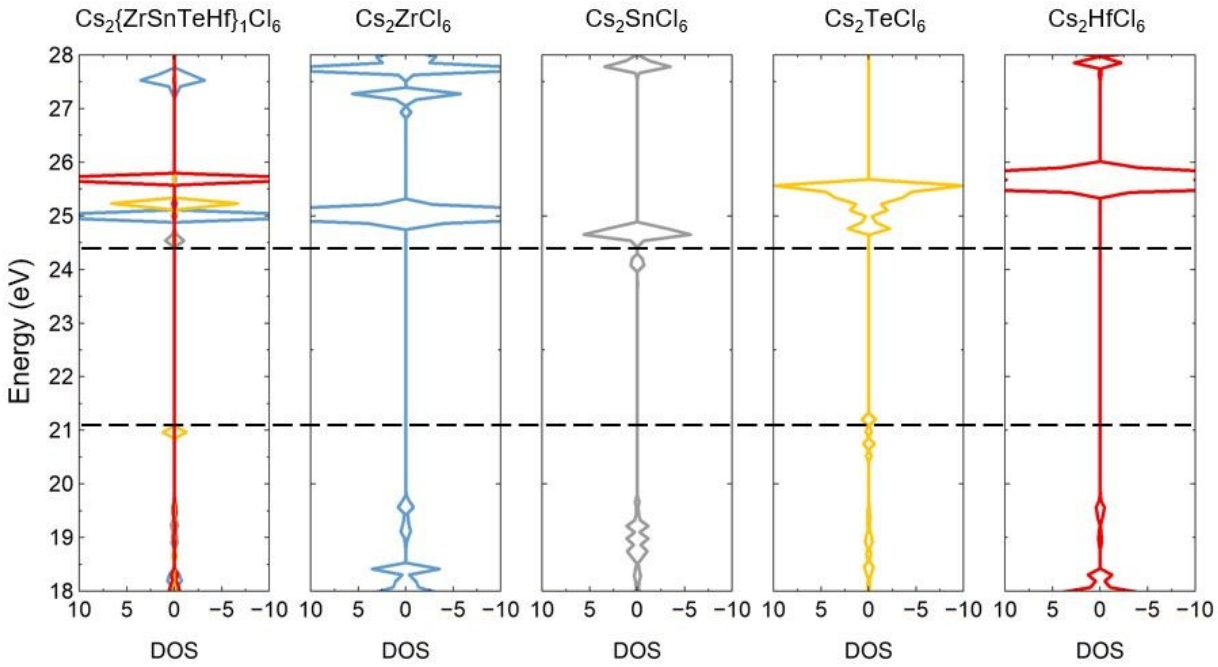

Figure 5 Alignment of the density of states for the B-site-mixed $Cs\{ZrSnTeHf\}_1Cl_6$ perovskite and its constituent pure perovskites: $CsZrCl_6$, $CsSnCl_6$, $CsTeCl_6$, and $CsHfCl_6$.

We then applied equation (3) to all B-site-mixed $Cs_2\{B_1B_2B_3B_4\}_1X_6$ and $Cs_2\{B_1B_2B_3B_4\}_1\{XX'\}_6$ perovskites, and Figure 6a shows the comparison between the predicted band gap from equation (3) and the DFT calculated band gap. We found that equation (3) can qualitatively predict the band gap of $Cs_2\{B_1B_2B_3B_4\}_1X_6$ and $Cs_2\{B_1B_2B_3B_4\}_1\{XX'\}_6$, especially when there are one or fewer paramagnetic metal ions (e.g., Re^{4+}, Os^{4+}, and Ir^{4+}). The red circles in Figure 6a correspond to $Cs_2\{B_1B_2B_3B_4\}_1X_6$ and $Cs_2\{B_1B_2B_3B_4\}_1\{XX'\}_6$ with multiple paramagnetic metal ions. Excluding these data points, the root-mean-square-error (RMSE) of the prediction is reduced from 0.79 eV to 0.67 eV (Figure 6b). The poor performance of equation (3) for $Cs_2\{B_1B_2B_3B_4\}_1X_6$ and $Cs_2\{B_1B_2B_3B_4\}_1\{XX'\}_6$ with multiple paramagnetic metal ions can be attributed to the complex interactions between the spins on the paramagnetic metal ions, which gives rise to different band edges from the pure perovskites.

Nanoscale Accepted Manuscript

View Article Online
DOI: 10.1039/D4NR05013D

Open Access Article. Published on 04 april 2025. Downloaded on 2025-04-13 20:33:42.
This article is licensed under a Creative Commons Attribution-NonCommercial 3.0 Unported Licence.

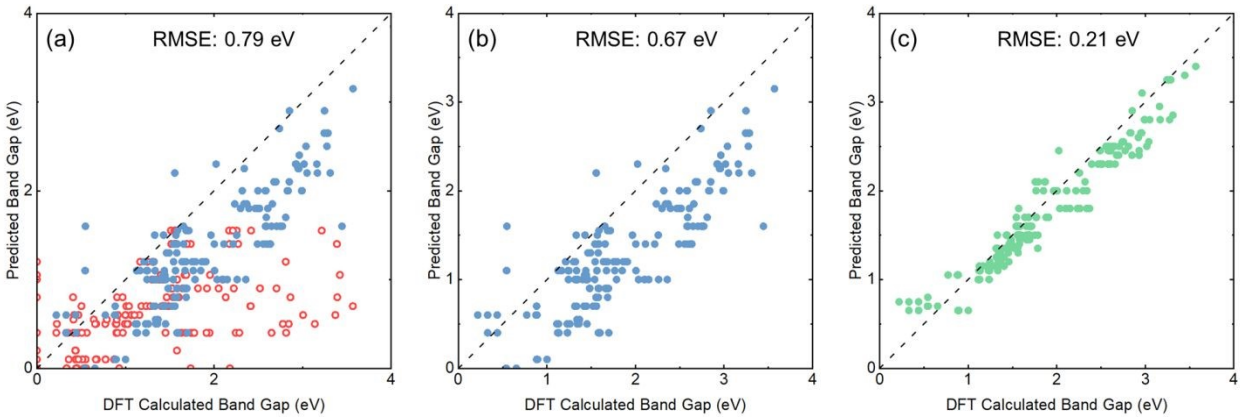

Figure 6 Comparison of the predicted and DFT calculated band gaps for $Cs_2\{B_1B_2B_3B_4\}_1X_6$ and $Cs_2\{B_1B_2B_3B_4\}_1\{XX'\}_6$ perovskites. (a) Predictions using pure perovskite band edges. Red circles represent perovskites with multiple paramagnetic metal ions (e.g., Re^{4+}, Os^{4+}, and Ir^{4+}). (b) Predictions using pure perovskite band edges with the red circles removed. (c) Predictions using band edges obtained from randomly chosen B-site-mixed perovskites.

One key approximation for equation (3) is that the positions of projected density of states are identical in B-site-mixed and pure perovskites. However, realistically, they are not exactly the same, as shown in Figures 4 and 5. Specially, we found that the VBM of the pure perovskite is ~ 0.2 eV higher than that of the B-site-mixed perovskite, while the CBM of the pure perovskite is ~ 0.2 eV lower than that of the B-site-mixed perovskite (Figure 5). Thus, the band gap predicted from equation (3) using the pure perovskite band edges are on average ~ 0.4 eV less than those from DFT calculations. Figure 6c shows that the RMSE is reduced from 0.67 eV to 0.21 eV, if the VBM and CBM values are obtained from randomly selected B-site-mixed perovskites instead of the pure perovskites. We have further analyzed the standard deviations of the VBM and CBM of the VODPs in various B-site-mixed perovskites and found them to be quite small (less than 0.1 eV). This suggests minimal fluctuations in the band edges of VODPs

Nanoscale Accepted Manuscript

View Article Online
DOI: 10.1039/D4NR05013D

Open Access Article. Published on 04 april 2025. Downloaded on 2025-04-13 20:33:42.
This article is licensed under a Creative Commons Attribution-NonCommercial 3.0 Unported Licence.

across various B-site-mixed perovskites, and using the average VBM and CBM of the VODPs for Equation 3 will not change the RMSE shown in Figure 6c significantly.

CONCLUSIONS

To summarize, we calculated the band gap and formation energy for 546 vacancy-ordered double perovskites, and found that the linear scaling relationship observed in Cs_2BX_6 and $Cs_2B\{XX'\}_6$ perovskites can be broken in medium-to-high-entropy perovskites. As a result, more than 90 $Cs_2\{B_1B_2B_3B_4\}_1X_6$ and $Cs_2\{B_1B_2B_3B_4\}_1\{XX'\}_6$ perovskites were predicted to be promising for solar absorbers with optimal band gap and high stability. We performed a detailed electronic structure analysis to understand the braking of the scaling relationship, and developed simple analytical equations to predict the band gap of B-site-mixed perovskites using the band gap of their constituent pure perovskites. This will significantly accelerate the design and discovery of novel medium/high-entropy perovskites with desired band gaps for both experimental and computational studies. In addition, the generated data from high throughput DFT calculations using the hybrid functional in this work will be beneficial for the community to further develop machine learning models for materials screening.

COMPUTATIONAL METHODS

Spin-polarized DFT calculations were performed as implemented in the Vienna ab initio simulation package (VASP 6.2.1).[50,51] The electron exchange-correlation was represented by the Perdew-Burke-Ernzerhof revised functional for solids (PBEsol) of generalized gradient approximation (GGA).[52] While the geometry optimizations were performed using the PBESol functional, the band gap and density of states calculations were performed using the hybrid

Nanoscale Accepted Manuscript

View Article Online
DOI: 10.1039/D4NR05013D

Open Access Article. Published on 04 april 2025. Downloaded on 2025-04-13 20:33:42.
This article is licensed under a Creative Commons Attribution-NonCommercial 3.0 Unported Licence.

HSE06 functional.[22] The ion-electron interaction was described with the projector augmented wave (PAW) method.[53] A cutoff energy of 500 eV was used for the plane-wave basis set. The energies were converged with a 1×10^{-5} eV tolerance, and the forces were optimized to within 0.01 eV/Å. The cubic phase of vacancy-ordered double perovskites was used, with a unit cell consisting of 8 Cs atoms, 4 B-site metals, and 24 halides. A 6 × 6 × 6 Monkhorst-Pack k-point grid was used for the geometry optimizations with the PBEsol functional, while a 3 × 3 × 3 Monkhorst-Pack k-point grid was used for the band gap calculations with the HSE06 hybrid functional. It is important to note that while the HSE06 functional is generally effective in predicting band gaps for many semiconductors, it has been shown to underestimate band gaps, particularly in halide perovskites.[54] Table S3 compares our calculated fundamental band gaps (VBM-CBM) from HSE06 with previous computational studies and experimentally measured optical band gaps. Our calculations are in excellent agreement with prior computational work. However, when compared to experimentally measured optical gaps, our results are consistently lower, which can be attributed to the dipole-allowed transition gaps discussed previously. Thus, determining the optical band gap and employing more accurate functionals, such as PBE0 or dielectric-dependent hybrid functionals, to better align with experimental results are important avenues for future research.

The formation energy of the pure perovskite $E_{form}(Cs_2BX_6)$ was calculated using the following equation:[55]

$$E_{form}(Cs_2BX_6) = E_{total}(Cs_2BX_6) - 2E(Cs) - E(B) - 6E(X) \quad (4)$$

where $E_{total}(Cs_2BX_6)$ is the total energy of the Cs_2BX_6 unit cell. E(Cs), E(B), and E(X) is the energy per atom for the corresponding elementary substances. For elements that have multiple allotropes, the reference state was chosen to be the form in which the element is most stable

Nanoscale Accepted Manuscript

View Article Online
DOI: 10.1039/D4NR05013D

Open Access Article. Published on 04 april 2025. Downloaded on 2025-04-13 20:33:42.
This article is licensed under a Creative Commons Attribution-NonCommercial 3.0 Unported Licence.

under 1 bar. The formation energy of the mixed perovskites was calculated in a similar way as equation (4). The initial atomic structures were obtained from materials projects.[56]

ACKNOWLEDGEMENTS

This material is based upon work supported as part of the Atomic-C2E project by the U.S. Department of Energy, Office of Science under Award Number DE-SC-0024716. This research used resources of the National Energy Research Scientific Computing Center, a DOE Office of Science User Facility supported by the Office of Science of the U.S. Department of Energy under Contract No. DE-AC02-05CH11231 using NERSC award BES-ERCAP0032102.

REFERENCES

(1) Szabó, G.; Park, N. G.; De Angelis, F.; Kamat, P. V. Are Perovskite Solar Cells Reaching the Efficiency and Voltage Limits? *ACS Energy Letters*. 2023, pp 3829–3831.

(2) Li, G.; Su, Z.; Canil, L.; Hughes, D.; Aldamasy, M. H.; Dagar, J.; Trofimov, S.; Wang, L.; Zuo, W.; Jerónimo-Rendon, J. J.; Byranvand, M. M.; Wang, C.; Zhu, R.; Zhang, Z.; Yang, F.; Nasti, G.; Naydenov, B.; Tsoi, W. C.; Li, Z.; Gao, X.; Wang, Z.; Jia, Y.; Unger, E.; Saliba, M.; Li, M.; Abate, A. Highly Efficient P-i-n Perovskite Solar Cells That Endure Temperature Variations. *Science* **2023**, *379*, 399–403.

(3) Li, M.; Jiao, B.; Peng, Y.; Zhou, J.; Tan, L.; Ren, N.; Ye, Y.; Liu, Y.; Yang, Y.; Chen, Y.; Ding, L.; Yi, C. High-Efficiency Perovskite Solar Cells with Improved Interfacial Charge Extraction by Bridging Molecules. *Adv. Mater.* **2024**, *36*, 2406532.

(4) Bati, A. S. R.; Zhong, Y. L.; Burn, P. L.; Nazeeruddin, M. K.; Shaw, P. E.; Batmunkh, M. Next-Generation Applications for Integrated Perovskite Solar Cells. *Communications Materials*. 2023.

(5) NREL. *Best Research-Cell Efficiency Chart*. https://www.nrel.gov/pv/cell-efficiency.html. (Accessed 24 October 2024).

(6) Kwak, J. Il; Lee, T. Y.; An, Y. J. Assessing the Potential Toxicity of Hazardous Material

Nanoscale Accepted Manuscript

View Article Online
DOI: 10.1039/D4NR05013D

Open Access Article. Published on 04 april 2025. Downloaded on 2025-04-13 20:33:42.
This article is licensed under a Creative Commons Attribution-NonCommercial 3.0 Unported Licence.

Released from Pb-Based Perovskite Solar Cells to Crop Plants. *J. Clean. Prod.* **2023**, *423*, 138856.

(7) Yue, Z.; Guo, H.; Cheng, Y. Toxicity of Perovskite Solar Cells. *Energies*. 2023, p 4007.

(8) Correa-Baena, J. P.; Saliba, M.; Buonassisi, T.; Grätzel, M.; Abate, A.; Tress, W.; Hagfeldt, A. Promises and Challenges of Perovskite Solar Cells. *Science*. 2017, pp 739–744.

(9) Rong, Y.; Hu, Y.; Mei, A.; Tan, H.; Saidaminov, M. I.; Seok, S. Il; McGehee, M. D.; Sargent, E. H.; Han, H. Challenges for Commercializing Perovskite Solar Cells. *Science*. 2018.

(10) Wang, D.; Wright, M.; Elumalai, N. K.; Uddin, A. Stability of Perovskite Solar Cells. *Sol. Energy Mater. Sol. Cells*. 2016, pp 255–275.

(11) Kim, G. Y.; Kim, K.; Kim, H. J.; Jung, H. S.; Jeon, I.; Lee, J. W. Sustainable and Environmentally Viable Perovskite Solar Cells. *EcoMat*. 2023, p e12319.

(12) Zhang, W.; Liu, H.; Yan, F.; Dong, B.; Wang, H. L. Recent Progress of Low-Toxicity Poor-Lead All-Inorganic Perovskite Solar Cells. *Small Methods*. 2024, p 2300421.

(13) Wu, C.; Zhang, Q.; Liu, Y.; Luo, W.; Guo, X.; Huang, Z.; Ting, H.; Sun, W.; Zhong, X.; Wei, S.; Wang, S.; Chen, Z.; Xiao, L. The Dawn of Lead-Free Perovskite Solar Cell: Highly Stable Double Perovskite Cs2AgBiBr6 Film. *Adv. Sci.* **2018**, *5*, 1700759.

(14) Zhu, Z.; Jiang, X.; Yu, D.; Yu, N.; Ning, Z.; Mi, Q. Smooth and Compact FASnI3 Films for Lead-Free Perovskite Solar Cells with over 14% Efficiency. *ACS Energy Lett.* **2022**, *7*, 2079–2083.

(15) Dureja, T.; Garg, A.; Bhalla, S.; Bhutani, D.; Khanna, A. Double Lead-Free Perovskite Solar Cell for 19.9% Conversion Efficiency: A SCAPS-1D Based Simulation Study. *Mater. Today Proc.*; 2022; Vol. 71, pp 239–242.

(16) Yang, J.; Manganaris, P.; Mannodi-Kanakkithodi, A. A High-Throughput Computational Dataset of Halide Perovskite Alloys. *Digit. Discov.* **2023**, *2*, 856–870.

(17) Morgan, E. E.; Kent, G. T.; Zohar, A.; O'Dea, A.; Wu, G.; Cheetham, A. K.; Seshadri, R. Hybrid and Inorganic Vacancy-Ordered Double Perovskites A2WCl6. *Chem. Mater.* **2023**, *35*, 7032–7038.

(18) Ju, M. G.; Chen, M.; Zhou, Y.; Garces, H. F.; Dai, J.; Ma, L.; Padture, N. P.; Zeng, X. C. Earth-Abundant Nontoxic Titanium(IV)-Based Vacancy-Ordered Double Perovskite

Nanoscale Accepted Manuscript

View Article Online
DOI: 10.1039/D4NR05013D

Open Access Article. Published on 04 april 2025. Downloaded on 2025-04-13 20:33:42.
This article is licensed under a Creative Commons Attribution-NonCommercial 3.0 Unported Licence.

Halides with Tunable 1.0 to 1.8 EV Bandgaps for Photovoltaic Applications. *ACS Energy Lett.* **2018**, *3*, 297–304.

(19) Zheng, K.; Chen, B.; Xie, L.; Li, X.; Lu, B.; Wang, M.; Wu, Y.; Jiang, T.; Zhang, F.; Li, X.; Wang, Y. Vacancy-Ordered Double Perovskite Rb2ZrCl6−xBrx: Facile Synthesis and Insight into Efficient Intrinsic Self-Trapped Emission. *Adv. Opt. Mater.* **2022**, *10*, 2101661.

(20) Vázquez-Fernández, I.; Mariotti, S.; Hutter, O. S.; Birkett, M.; Veal, T. D.; Hobson, T. D. C.; Phillips, L. J.; Danos, L.; Nayak, P. K.; Snaith, H. J.; Xie, W.; Sherburne, M. P.; Asta, M.; Durose, K. Vacancy-Ordered Double Perovskite Cs2TeI6Thin Films for Optoelectronics. *Chem. Mater.* **2020**, *32*, 6676–6684.

(21) Ye, X.; Liu, A.; Gao, L.; Zhang, C.; Yan, L.; Wen, S.; Ma, T. Computational Screening of Cs Based Vacancy-Ordered Double Perovskites for Solar Cell and Photocatalysis Applications. *EcoMat* **2023**, *5*, e12295.

(22) Cucco, B.; Bouder, G.; Pedesseau, L.; Katan, C.; Even, J.; Kepenekian, M.; Volonakis, G. Electronic Structure and Stability of Cs2TiX6and Cs2ZrX6(X = Br, I) Vacancy Ordered Double Perovskites. *Appl. Phys. Lett.* **2021**, *119*.

(23) Liu, A.; Zhu, H.; Reo, Y.; Kim, M. G.; Chu, H. Y.; Lim, J. H.; Kim, H. J.; Ning, W.; Bai, S.; Noh, Y. Y. Modulation of Vacancy-Ordered Double Perovskite Cs2SnI6 for Air-Stable Thin-Film Transistors. *Cell Reports Phys. Sci.* **2022**, *3*, 100812.

(24) Faizan, M.; Wang, X.; Abdelmohsen, S. A. M.; Bhamu, K. C.; Sappati, S.; Laref, A.; Muhammad, N.; Mushtaq, M.; Abdelbacki, A. M. M.; Khenata, R. Understanding the Electronic Structure and Optical Properties of Vacancy-Ordered Double Perovskite A2BX6for Optoelectronic Applications. *Energy and Fuels* **2022**, *36*, 7065–7074.

(25) Folgueras, M. C.; Jiang, Y.; Jin, J.; Yang, P. High-Entropy Halide Perovskite Single Crystals Stabilized by Mild Chemistry. *Nature* **2023**, *621*, 282–288.

(26) Wang, X.; Yang, J.; Wang, X.; Faizan, M.; Zou, H.; Zhou, K.; Xing, B.; Fu, Y.; Zhang, L. Entropy-Driven Stabilization of Multielement Halide Double-Perovskite Alloys. *J. Phys. Chem. Lett.* **2022**, *13*, 5017–5024.

(27) Jiang, S.; Hu, T.; Gild, J.; Zhou, N.; Nie, J.; Qin, M.; Harrington, T.; Vecchio, K.; Luo, J. A New Class of High-Entropy Perovskite Oxides. *Scr. Mater.* **2018**, *142*, 116–120.

(28) Wang, T.; Chen, H.; Yang, Z.; Liang, J.; Dai, S. High-Entropy Perovskite Fluorides: A

Nanoscale Accepted Manuscript

View Article Online
DOI: 10.1039/D4NR05013D

New Platform for Oxygen Evolution Catalysis. *J. Am. Chem. Soc.* **2020**, *142*, 4550–4554.

(29) Stratulat, A. M.; Tantardini, C.; Azizi, M.; Altalhi, T.; Levchenko, S. V.; Yakobson, B. I. Electronic Properties of Zn2V(1-x)NbxN3 Alloys to Model Novel Materials for Light-Emitting Diodes. *J. Phys. Chem. Lett.* **2023**, *14*, 9118–9125.

(30) Ning, Y.; Pu, Y.; Wu, C.; Chen, Z.; Zhang, X.; Zhang, L.; Wang, B. Design Strategy of High-Entropy Perovskite Energy-Storage Ceramics: A Review. *J. Eur. Ceram. Soc.*. 2024, pp 4831–4843.

(31) Nguyen, T. X.; Liao, Y. C.; Lin, C. C.; Su, Y. H.; Ting, J. M. Advanced High Entropy Perovskite Oxide Electrocatalyst for Oxygen Evolution Reaction. *Adv. Funct. Mater.* **2021**, *31*, 2101632.

(32) Amiri, A.; Shahbazian-Yassar, R. Recent Progress of High-Entropy Materials for Energy Storage and Conversion. *J. Mater. Chem. A*. 2021, pp 782–823.

(33) Wu, D.; Kusada, K.; Yamamoto, T.; Toriyama, T.; Matsumura, S.; Kawaguchi, S.; Kubota, Y.; Kitagawa, H. Platinum-Group-Metal High-Entropy-Alloy Nanoparticles. *J. Am. Chem. Soc.* **2020**, *142*, 13833–13838.

(34) Karim, M. M. S.; Ganose, A. M.; Pieters, L.; Winnie Leung, W. W.; Wade, J.; Zhang, L.; Scanlon, D. O.; Palgrave, R. G. Anion Distribution, Structural Distortion, and Symmetry-Driven Optical Band Gap Bowing in Mixed Halide Cs2SnX6 Vacancy Ordered Double Perovskites. *Chem. Mater.* **2019**, *31*, 9430–9444.

(35) Colella, S.; Mosconi, E.; Fedeli, P.; Listorti, A.; Gazza, F.; Orlandi, F.; Ferro, P.; Besagni, T.; Rizzo, A.; Calestani, G.; Gigli, G.; De Angelis, F.; Mosca, R. MAPbI3-XClx Mixed Halide Perovskite for Hybrid Solar Cells: The Role of Chloride as Dopant on the Transport and Structural Properties. *Chem. Mater.*; 2013; Vol. 25, pp 4613–4618.

(36) Unger, E. L.; Bowring, A. R.; Tassone, C. J.; Pool, V. L.; Gold-Parker, A.; Cheacharoen, R.; Stone, K. H.; Hoke, E. T.; Toney, M. F.; McGehee, M. D. Chloride in Lead Chloride-Derived Organo-Metal Halides for Perovskite-Absorber Solar Cells. *Chem. Mater.* **2014**, *26*, 7158–7165.

(37) Chae, J.; Dong, Q.; Huang, J.; Centrone, A. Chloride Incorporation Process in CH3NH3PbI3-XClx Perovskites via Nanoscale Bandgap Maps. *Nano Lett.* **2015**, *15*, 8114–8121.

(38) Xiao, H. J.; Li, H.; Chang, L.; Zhang, H. X.; Xuan, H. C. Theoretical Prediction for the

Open Access Article. Published on 04 april 2025. Downloaded on 2025-04-13 20:33:42.
This article is licensed under a Creative Commons Attribution-NonCommercial 3.0 Unported Licence.

Nanoscale Accepted Manuscript

View Article Online
DOI: 10.1039/D4NR05013D

Open Access Article. Published on 04 april 2025. Downloaded on 2025-04-13 20:33:42.
This article is licensed under a Creative Commons Attribution-NonCommercial 3.0 Unported Licence.

Band Gap of Semiconductor Nanoparticles as Function of Bond Number. *Mater. Chem. Phys.* **2016**, *184*, 285–290.

(39) Smith, A. M.; Nie, S. Semiconductor Nanocrystals: Structure, Properties, and Band Gap Engineering. *Acc. Chem. Res.* **2010**, *43*, 190–200.

(40) Maughan, A. E.; Ganose, A. M.; Scanlon, D. O.; Neilson, J. R. Perspectives and Design Principles of Vacancy-Ordered Double Perovskite Halide Semiconductors. *Chemistry of Materials*. 2019, pp 1184–1195.

(41) Kirchartz, T.; Rau, U. What Makes a Good Solar Cell? *Adv. Energy Mater.* **2018**, *8*, 1703385.

(42) Zhao, X. H.; Wei, X. N.; Tang, T. Y.; Gao, L. K.; Xie, Q.; Lu, L. M.; Tang, Y. L. First-Principles Study on the Structural, Electronic and Optical Properties of Vacancy-Ordered Double Perovskites Cs2PtI6 and Rb2PtI6. *Opt. Mater. (Amst).* **2021**, *114*, 110952.

(43) Yang, S.; Wang, L.; Zhao, S.; Liu, A.; Zhou, Y.; Han, Q.; Yu, F.; Gao, L.; Zhang, C.; Ma, T. Novel Lead-Free Material Cs2PtI6with Narrow Bandgap and Ultra-Stability for Its Photovoltaic Application. *ACS Appl. Mater. Interfaces* **2020**, *12*, 44700–44709.

(44) Maughan, A. E.; Ganose, A. M.; Bordelon, M. M.; Miller, E. M.; Scanlon, D. O.; Neilson, J. R. Defect Tolerance to Intolerance in the Vacancy-Ordered Double Perovskite Semiconductors Cs2SnI6 and Cs2TeI6. *J. Am. Chem. Soc.* **2016**, *138*, 8453–8464.

(45) Kavanagh, S. R.; Savory, C. N.; Liga, S. M.; Konstantatos, G.; Walsh, A.; Scanlon, D. O. Frenkel Excitons in Vacancy-Ordered Titanium Halide Perovskites (Cs2TiX6). *J. Phys. Chem. Lett.* **2022**, *13*, 10965–10975.

(46) Cucco, B.; Katan, C.; Even, J.; Kepenekian, M.; Volonakis, G. Fine Structure of Excitons in Vacancy-Ordered Halide Double Perovskites. *ACS Mater. Lett.* **2023**, *5*, 52–59.

(47) Saura-Múzquiz, M.; Avdeev, M.; Brand, H. E. A.; Kennedy, B. J. Structural and Magnetic Properties of Some Vacancy-Ordered Osmium Halide Perovskites. *Inorg. Chem.* **2022**, *61*, 15961–15972.

(48) Zhang, Y.; Lin, L.-F.; Moreo, A.; Dagotto, E.; Phys Lett, A. Electronic and Magnetic Properties of Quasi-One-Dimensional Osmium Halide OsCl 4 □ Special Collection: One-Dimensional van Der Waals Materials Preparation of Osmium Targets with Carbon Backing Structure and Mechanical Properties of Osmium Carbide: First-Principles Calculations Investigation of Osmium Carbides with Various Stoichiometries: First-

Nanoscale Accepted Manuscript

View Article Online
DOI: 10.1039/D4NR05013D

Principles Calculations. *Appl. Phys. Lett* **2022**, *120*, 23101.

(49) Song, Y.; Pan, J.; Zhang, Y.-F.; Yang, H.; Du, S. Monolayer Iridium Sulfide Halides with High Mobility Transport Anisotropy and Highly Efficient Light Harvesting. *J. Phys. Chem. Lett. 2021* **2021**, *12*, 6007–6013.

(50) Kresse, G.; Hafner, J. Ab Initio Molecular Dynamics for Liquid Metals. *Phys. Rev. B* **1993**, *47*, 558–561.

(51) Kresse, G.; Furthmüller, J. Efficiency of Ab-Initio Total Energy Calculations for Metals and Semiconductors Using a Plane-Wave Basis Set. *Comput. Mater. Sci.* **1996**, *6*, 15–50.

(52) Perdew, J. P.; Ruzsinszky, A.; Csonka, G. I.; Vydrov, O. A.; Scuseria, G. E.; Constantin, L. A.; Zhou, X.; Burke, K. Restoring the Density-Gradient Expansion for Exchange in Solids and Surfaces. *Phys. Rev. Lett.* **2008**, *100*.

(53) Joubert, D. From Ultrasoft Pseudopotentials to the Projector Augmented-Wave Method. *Phys. Rev. B - Condens. Matter Mater. Phys.* **1999**, *59*, 1758–1775.

(54) Wang, H.; Tal, A.; Bischoff, T.; Gono, P.; Pasquarello, A. Accurate and Efficient Band-Gap Predictions for Metal Halide Perovskites at Finite Temperature. *npj Comput. Mater.* **2022**, *8*, 1–13.

(55) Zhao, X. H.; Wei, X. N.; Tang, T. Y.; Xie, Q.; Gao, L. K.; Lu, L. M.; Hu, D. Y.; Li, L.; Tang, Y. L. Theoretical Prediction of the Structural, Electronic and Optical Properties of Vacancy-Ordered Double Perovskites Tl2TiX6 (X = Cl, Br, I). *J. Solid State Chem.* **2022**, *305*, 122684.

(56) Jain, A.; Ong, S. P.; Hautier, G.; Chen, W.; Richards, W. D.; Dacek, S.; Cholia, S.; Gunter, D.; Skinner, D.; Ceder, G.; Persson, K. A. Commentary: The Materials Project: A Materials Genome Approach to Accelerating Materials Innovation. *APL Materials*. 2013, p 11002.

Open Access Article. Published on 04 april 2025. Downloaded on 2025-04-13 20:33:42.
This article is licensed under a Creative Commons Attribution-NonCommercial 3.0 Unported Licence.

Nanoscale Accepted Manuscript

View Article Online
DOI: 10.1039/D4NR05013D

Data Availability Statement:

All data from this work will be shared, including the data needed to reproduce the results and the raw data from VASP calculations. The data will be shared on the open-source repository Figshare. They will be made available immediately following the publication of the work.

Open Access Article. Published on 04 april 2025. Downloaded on 2025-04-13 20:33:42.
This article is licensed under a Creative Commons Attribution-NonCommercial 3.0 Unported Licence.

Nanoscale Accepted Manuscript